Available online at www.sciencedirect.com
SCIENCE DIRECT®
Pergamon
Materials Research Bulletin 38 (2003) 647–656
Materials Research Bulletin
www.elsevier.com/locate/matresbu

Anode behaviors of aluminum antimony synthesized by mechanical alloying for lithium secondary battery

H. Honda, H. Sakaguchi, Y. Fukuda, T. Esaka*

Department of Materials Science, Faculty of Engineering, Tottori University, Minami 4-101, Koyama-cho, Tottori 680-8552, Japan

Received 28 June 2002; received in revised form 6 November 2002; accepted 17 December 2002

Abstract

AlSb was synthesized as an anode active material for lithium secondary battery using mechanical alloying (MA). Electrochemical performance was examined on the electrodes of AlSb synthesized with different MA time. The first charge (lithium-insertion) capacity of the AlSb electrodes decreased with increasing the MA time. The discharge capacity on repeating charge–discharge cycle, however, did not show the same dependence. The electrode, consisting of the 20 h MA sample exhibited the longest charge–discharge life cycle, suggesting that there is the optimum degree of internal energy derived from the strain and/or the amorphization due to mechanical alloying. These results were evaluated using ex situ X-ray diffraction and differential scanning calorimetry.

Keywords: Intermetallic compounds; Mechanical alloying; Electrochemical property; Energy storage

1. Introduction

Carbon materials are commercially used as negative electrode materials in lithium secondary batteries, but higher capacity alternatives with lower irreversible capacities are still necessary. Although several binary lithium alloys were investigated, their capacity retention during cycling was limited by large volume changes of the alloys [1–4]. In the recent search on anode materials, there has been a considerable interest in intermetallic compounds [5–21], such as Sn_xFe [6–8], Cu_6Sn_5 [9–12], and Sn/SnSb [13–15]. Although these compounds decompose during lithium insertion down to 0 V to form Li–Sn alloy, they have the advantage of high capacity and relatively excellent reversibility. In similar research for materials having larger capacity, several Sb-based compounds, $CoSb_3$ [16], $TiSb_2$ [17], Zn_4Sb_3 [18,19], $CoFe_3Sb_{12}$ [19], etc. were also investigated. In the most of antimonides exhibited large

* Corresponding author. Tel.: +81-857-31-5264; fax: +81-857-31-526.
E-mail address: esaka@chem.tottori-u.ac.jp (T. Esaka).

0025-5408/03/$ – see front matter
doi:10.1016/S0025-5408(03)00003-5

capacity, the inactive component was extruded from the compound each on the first cycle, and the original compound was not restored during cycling.

Besides these compounds, intermetallic compounds, Mg_2Ge [22–26] and Mg_2Sn [27,28], appeared to be more attractive materials. Especially, in the former case, lithium atoms (or ions) could be inserted electrochemically into the lattice within the defined potential ranges, to form a solid solution. We have already shown, from X-ray diffraction (XRD) and neutron scattering experiments, that lithium atoms (or ions) are accommodated to interstitial sites in the Mg_2Ge lattice [26]. Furthermore, we have discussed the relationship between the anode characteristics and the internal energies of Mg_2Ge synthesized by mechanical alloying (MA) [25], and reported that the charge–discharge performance of the electrodes was influenced by the internal energy originated from the crystallinity change and/or the introduction of lattice strain. Therefore, the compound is found to have the optimum internal energy for the best electrode performance.

Recently, Vaughey et al. [29] and Dahn and coworkers [30] have proposed a new intermetallic compound, InSb, with a ZnS-type structure, which is characterized to have so large interstitial sites for lithium insertion in its crystal lattice. According to their report, although the amounts of inserted lithium were only 0.27 lithium atoms per InSb, i.e. about 5% of the overall capacity, lithium could be taken in the open framework structure followed by indium extraction. Subsequently, the electrode reacts with further 2.73 lithium atoms, which results in the formation of Li_3Sb and indium. And finally, the indium can react with further lithium. However, if the charge–discharge reactions of these Li/InSb cells are taken above 0.5 V, the electrode reaction of InSb is reversible.

AlSb has the same structure as InSb, and the electrode reaction of the compound is expected to proceed in a similar manner as the InSb electrode. Earlier work revealed that AlSb metallurgically obtained reacts to lithium with large lattice expansion [22], and that particles of the compound disintegrate on repeating insertion–extraction of lithium. This might be a serious drawback for its practical use as an electrode of rechargeable battery. Considering that the lattice expansion varies the internal energy due to the introduction of strain above as mentioned in Mg_2Ge, the appropriate internal energy given initially may make the lattice expansion moderate due to the relaxation of stress on lithium insertion. Up to date, however, no research has carried out on AlSb as to the relation between the discharge capacity and the degree of internal energy. In the present work, we were going to synthesize AlSb by the MA technique, and the electrode performance was investigated on the resultant samples.

2. Experimental

A mixture of elemental Al (Goodfellow Cambridge, >99.5% pure, particle size ca. 400 μm) and Sb (Goodfellow Cambridge, >99.2% pure, particle size ca. 50 μm) powders were put in a stainless steel vessel (80 ml) together with five balls (∅ 15). The Al/Sb atomic ratio was 1.0, and the weight ratio of the balls to the sample was about 15:1. The vessel used was sealed with an O-ring to keep an atmosphere of dry argon gas (>99.99% pure). Milling was done using a high-energy planetary ball mill (Itoh, LP-4/2) at 300 rpm and at room temperature.

To identify phases of mechanically alloyed samples, X-ray diffraction (Shimadzu, XRD-6000) was carried out using Ni-filtered CuKα radiation at a 2θ scan of $2^\circ\ min^{-1}$. The thermal stability of the samples was examined by means of differential scanning calorimetry (DSC) with a Shimadzu DSC-50 in a flow of argon at a heating rate of $0.083\ ^\circ C\ s^{-1}$. The chemical composition and impurities were

determined with ICP emission spectroscope (Shimadzu, ICPS-5000). The sample powders obtained were observed by scanning electron microscopy (SEM) in order to know the sample morphology and the particle size distribution. The particle size distribution was also obtained by a laser diffraction method (Shimadzu, SALD-2100). To break down larger aggregates to smaller ones, the powder suspensions have been treated with ultrasound before and during the measurement.

Electrochemical performance of an electrode was estimated with a three-electrode cell. The construction of a working electrode was as follows: AlSb (MA sample), scale-shape graphite (SFG6), and poly(vinylidenefluoride) (PVDF) were mixed in the weight ratio of 75:20:5 and was smeared on a copper mesh (1 cm × 1 cm). SFG6 and PVDF were a conductive material and a binder, respectively. In the test cell, both counter and reference electrodes were 1 mm thick lithium metal sheets (Rare Metallic, 99.9% pure). One molar $LiClO_4$ dissolved in propylene carbonate (PC) (Kishida Chemical) was used as an electrolyte. The electrode performance was evaluated galvanostatically at the current density of 0.2 mA cm^{-2} (10 mA g^{-1}) for both charge and discharge at room temperature. Cyclic voltammetric measurements were also carried out with the three-electrode cell at the scan rate of 0.1 mV s^{-1}.

To clarify the electrode reaction, ex situ XRD measurements were done for the mixed active materials obtained by stopping the lithium insertion–extraction at the various voltages. In each case, the testing sample was peeled off from the copper current collector and was dried for overnight in vacuo.

3. Results and discussion

Fig. 1 shows XRD patterns of the mechanically alloyed products using elemental Al and Sb as starting materials. After 5 h milling, the diffraction pattern corresponded to a single cubic phase

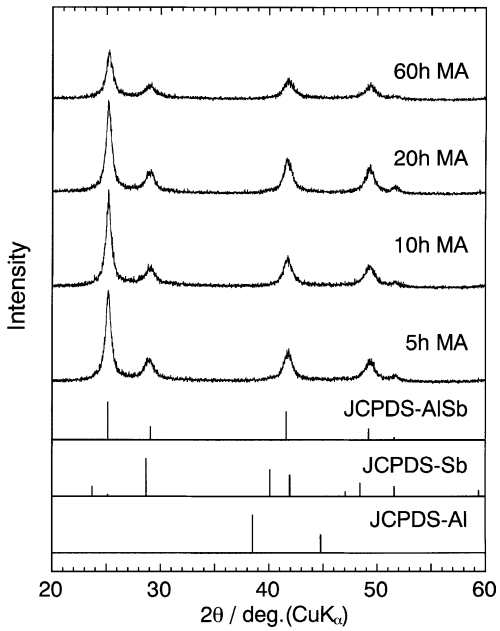

Fig. 1. Change in XRD patterns of elemental Al–Sb mixture with the mechanical alloying time.

(JCPDS-AlSb) with a zinc-blende-type structure and no diffraction peak of the starting materials was observed. Prolonged MA treatments resulted in no obvious change in the diffraction pattern until 20 h at last. However, broadening of the diffraction peaks was observed for 60 h MA, indicating reduction of particle size and decrease in crystallinity followed by increase in lattice strain. From the ICP measurement, the sample mechanically alloyed for 10 h had a composition of $Al_{0.96}SbFe_{0.05}Cr_{0.01}$-$Ni_{0.01}$, which denoted that the sample has prepared almost stoichiometrically, although some contamination was derived from the stainless steel vessel and balls.

The distribution of aggregate size is shown in Fig. 2; the largest frequency was obtained at 0.1–0.2 μm aggregate size range on the 10 and 20 h MA samples, while that shifted to lower than 1 μm on the 60 h MA sample. Fig. 3 displays the SEM images of AlSb powders synthesized with the different MA times. Larger aggregates composed of fine particles are obviously seen for all samples. Especially, the 60 h MA sample forms large aggregates. The DSC curves on the various MA samples (Fig. 4) had broad exothermic peaks centered around 250 °C. Considering that the peak was irreversible ones, the peak area was getting large with the MA time, and no thermogravimetric change was observed corresponding to the peaks, the exothermic peaks are not attributable to oxidation of the compounds. After the DSC measurements, the XRD peak assigned to an AlSb phase obviously increased in intensity

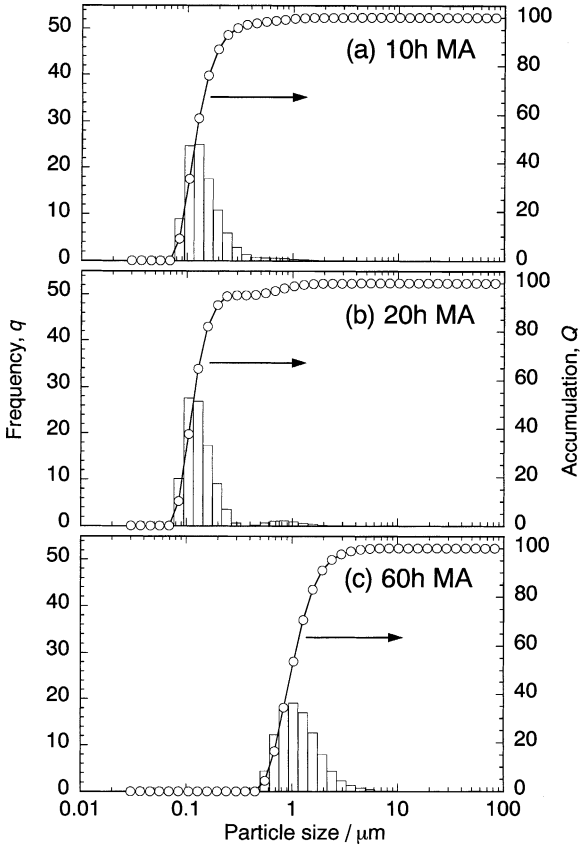

Fig. 2. Particle size distributions of AlSb synthesized with the different MA times. The parts a, b and c correspond to those in Fig. 3.

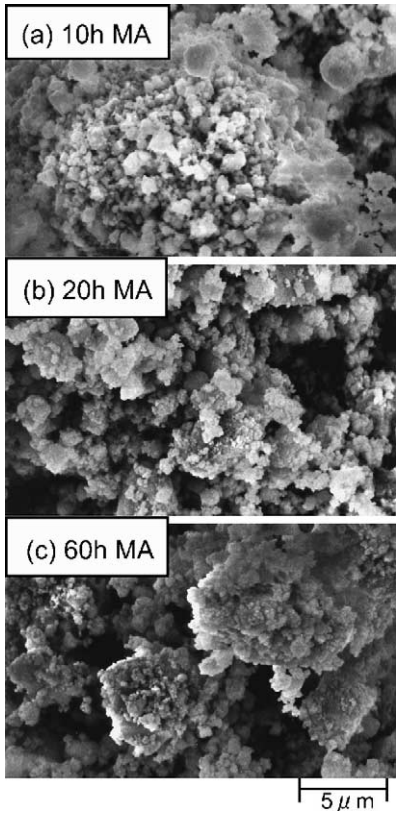

Fig. 3. SEM images of AlSb synthesized with the different MA times.

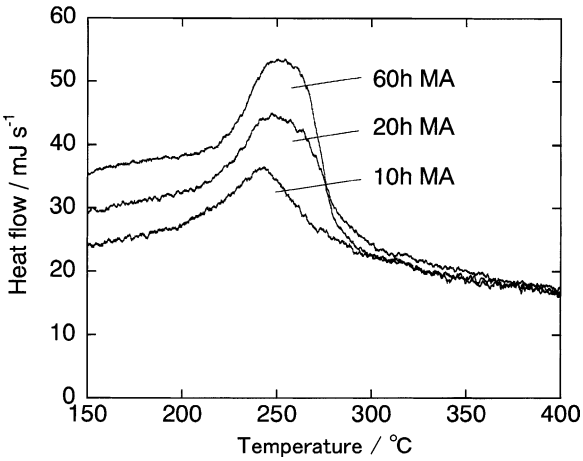

Fig. 4. DSC curves of AlSb synthesized with the different MA times.

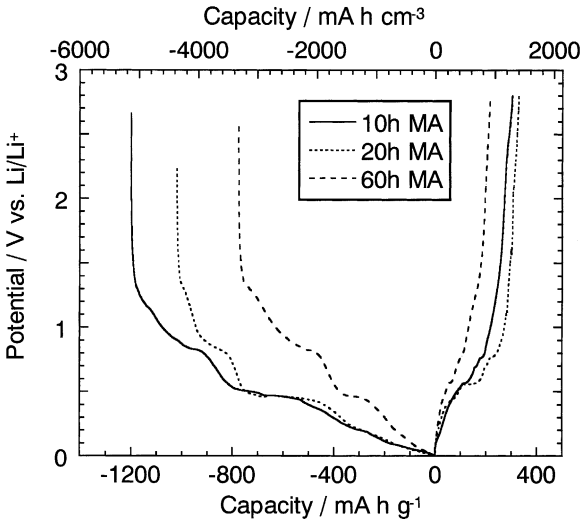

Fig. 5. The first charge–discharge curves for the electrodes of AlSb synthesized with the different MA times.

for all of the MA samples. Consequently, the exothermic peaks appear to be caused by crystallization and/or release of internal strain. The exothermic calorific value estimated from the peak areas were 975, 1289 and 1508 J g^{-1} for the 10, 20 and 60 h MA samples, respectively. Accordingly, AlSb synthesized by the MA method has the various degree of internal energy originated from the crystallinity change and/or the introduction of lattice strain.

Fig. 5 illustrates charge–discharge curves of the AlSb electrodes synthesized with the different MA time. The first charge (lithium-insertion) capacity of the electrode was ca. 1200 mAh g^{-1}, suggesting AlSb has a large latent power density as an anode material for lithium batteries. On the other hand, the first discharge (lithium-extraction) capacity was ca. 300 mAh g^{-1}, which may not be so large. However, if the discharge capacity was shown volumetrically considering the alloy density of ca. 4.3 g cm^{-3}, that would be ca. 1290 mAh cm^{-3}, which is about 1.5 times larger than that of the carbon materials. As increasing the MA time from 10 to 60 h, the charge capacity decreased monotonously. On the contrary, the largest discharge capacity was observed for the 20 h MA sample, suggesting that there is an optimum MA time for the anode material.

To check the phase changes during electrochemical lithiation, XRD was carried out on the samples obtained at various lithium-insertion steps (Fig. 6). A little broadening of the diffraction peaks was observed during the initial lithium insertion process down to 0 V, indicating pulverization of the sample particles and/or introduction of lattice strain. In addition, the diffraction peaks slightly shifted toward the lower angle. This suggests a possibility that AlSb reacted with lithium and formed a solid solution. When the potential reached to 0 V, however, the Li_3Sb was confirmed as a new phase, meaning the decomposition of AlSb. As for the lithium extraction process, the discharge up to 2.8 V, the Li_3Sb phase was found to disappear and the AlSb phase was restructured.

The observed high lithium-insertion capacity is too high to be explained by the formation of solid solution and Li_3Sb. Assuming that lithium accommodates the octahedral sites (4*b*) in AlSb, one lithium atom reacts with a formula unit of AlSb. The formation of Li_3Sb at the potential reached to 0 V should be accompanied by the formation of metallic aluminum. In the case of pure aluminum, the formation of

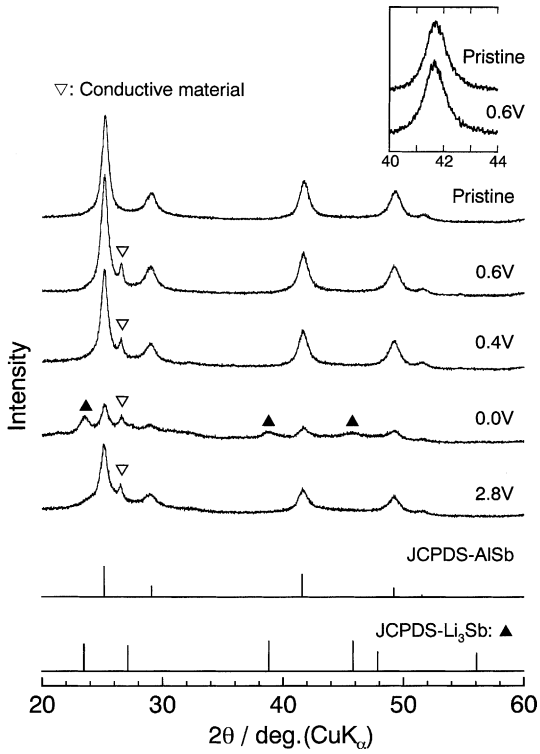

Fig. 6. XRD patterns of AlSb at various lithiated steps. Each datum was obtained at the first charge–discharge cycle.

LiAl takes place at around 300 mV versus Li [31], and the charge curve contains at least one plateau below 300 mV which could correspond to that reaction (Fig. 5). At 0 V, the presence of Al and LiAl phase was not revealed by XRD patterns. Both domains may be too small to be identified in the XRD spectra.

Assuming a reaction mechanism with the formation of Li_3Sb and LiAl the theoretical capacity is 721 mAh g^{-1}. The large irreversible capacity at the first cycle indicates that a large amount of lithium is irreversibly inserted into the electrode. Several side reactions can be considered to explain the observed irreversible capacity loss. As a case of the non-graphitizable (hard) carbon electrode, many lithium ions could be inserted into defect sites. Although this is only one instance among many, MA-methods would be introduced some defect sites into AlSb compounds. A part of the host atoms at defect sites within the bulk or on the surface of the electrode bound tightly to lithium ions. In the present case, lithium ions are in the stable site in AlSb, and hardly extract in the discharge process.

The cyclic voltammogram of the AlSb electrode shown in Fig. 7 compared with that of the metallic Sb and Al electrode. A large cathodic current peak appeared at the range of 1.8–0.5 V versus Li/Li^+ in the first reduction half-cycle for the AlSb electrode, but not for the metallic Sb and Al electrode. There was also difference in the profile of the oxidation process. These results suggested that the lithium insertion reaction of AlSb was not only based on the formation and the decomposition of Li–Sb and Li–Al alloy but also on lithium absorption into the interstitial sites of AlSb lattice. The voltammogram obtained at the following cycle shows the poor cyclability of the AlSb electrode. The irreversible

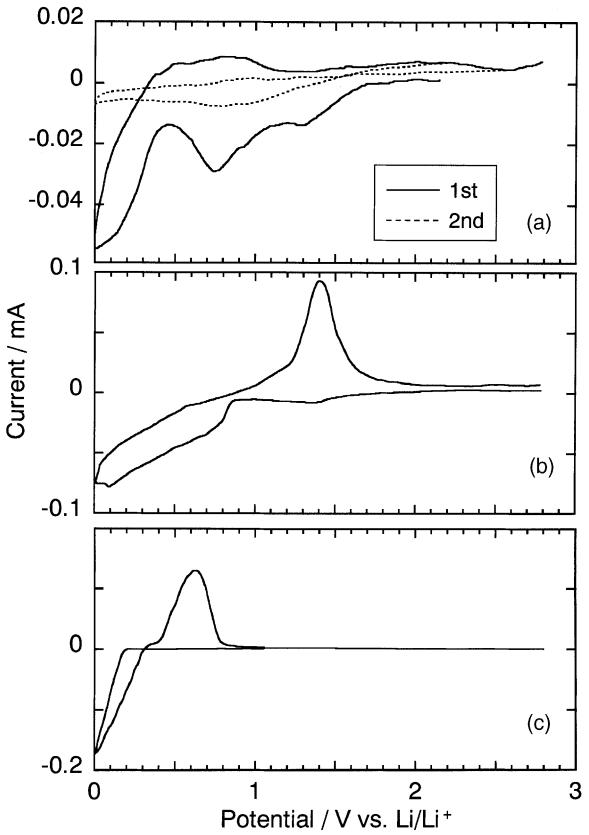

Fig. 7. Cyclic voltammograms (0.1 mV s^{-1}) for the electrode consisting of (a) AlSb, (b) metallic Sb and (c) metallic Al.

current peak around 1.3 V of reduction process may be caused by the irreversible side reactions. The current peak based on the formation of Li–Sb and Li–Al alloy also falls into decay, especially in the range of 0.4–0 V of the reduction process. The XRD pattern of the fully lithiated sample, presented in Fig. 6, still reveals the presence of AlSb phase, although these patterns may be derived from solid solution, Li_xAlSb, of which interstitial sites were occupied by lithium. The volume of the electrode would be changed violently during the formation of Li–Sb and Li–Al alloy, which would lead to the crack of the packed electrode powders. These results mean that some powders of the electrode must have lost their electrochemical activity during the charge–discharge cycle, which also explain the large irreversibility.

Fig. 8 displays the relationship between discharge capacity and charge–discharge cycle number for the AlSb electrode. The best performance was obtained on the electrode consisting of the 20 h MA sample. Accordingly, there appears to be the optimum internal energy to extend the cycle life on the AlSb electrode as on the Mg_2Ge electrode previously reported [25]. The cycle life, however, must be too short for the practical use, which would be caused by both decomposition of AlSb and formation of Li_3Sb as mentioned above. Vaughey et al. [29] have reported that the charge–discharge reversibility of the AlSb electrode was improved by the charge–discharge cycling carried out in the limited range from the potential of 0.5 to 1.2 V. This appears to inhibit Li_3Sb formation, which should occur at less than 0.5 V.

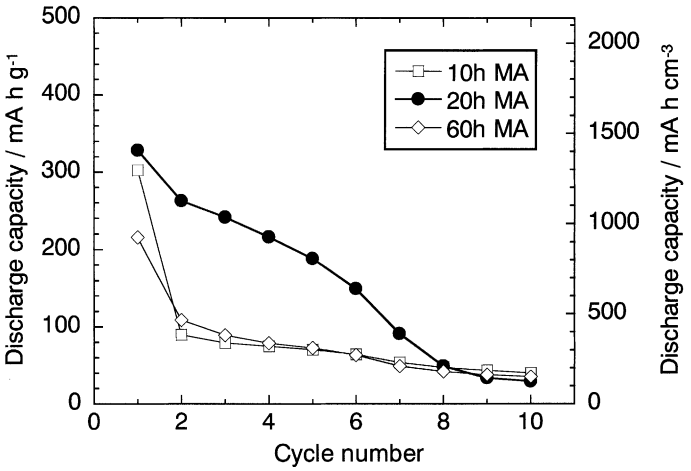

Fig. 8. Dependence of discharge capacity on charge–discharge cycling for the AlSb electrodes.

Considering this result and Fig. 8, cyclability of the relevant electrode could be improved not only by applying the optimum internal energy, but also by restricting the potential range for charge and discharge.

In our previous study of the Mg_2Ge electrodes, samples with various internal energies were also obtained by varying MA time from 25 to 100 h. XRD peaks of the samples got broad with the MA time, indicating a decrease in crystallinity and/or an increase in lattice strain. As for the distribution of aggregate size, the largest frequency was obtained at the aggregate with sizes of 0.5–1 μm, and did not depend on the MA time. The DSC curves on the various MA samples had a broad exothermic peak, as in the case of AlSb in this article. The heats estimated from the peaks were 305, 368, 599 and 772 J g^{-1} for 25, 40, 80 and 100 h MA samples, respectively. The first discharge capacity of the Mg_2Ge electrode decreased with increasing MA time. The decrement of discharge capacity with repeating charge–discharge cycle, however, did not correspond to the order. The sample prepared by MA for 40 h exhibited the longest cycle life, suggesting that the charge–discharge characteristics were found to be influenced by the internal energy originated from the crystallinity change and/or the introduction of lattice strain. Then, we proposed that control of the optimum internal energy in the intermetallic compounds is necessary to obtain the best electrochemical performance, since the appropriate internal energy must make the lattice expansion moderate due to relaxation of stress at lithium insertion. Although AlSb synthesized with various MA time has different grades of agglomerations for three samples, the present results on the AlSb electrode are considered to support the concept.

4. Conclusions

The lithium storage intermetallic compound, AlSb, with the different internal energy was synthesized by mechanical alloying. The ex situ XRD results suggest a possibility that AlSb reacted with lithium and formed a solid solution on lithium insertion. When the potential reached down to 0 V, the electrode reaction was based on the formation and decomposition of lithium antimonides, meaning the decomposition of AlSb. However, the AlSb phase was restructured at the lithium extraction process. The largest discharge capacity was observed for the 20 h MA sample at the first cycle; ca. 300 mAh g^{-1}

for gravimetric capacity and ca. 1290 mAh cm^{-3} for volumetric capacity. The electrode consisting of the 20 h MA sample exhibited the best cycle life among the present AlSb samples obtained with various MA time from 10 to 60 h. This suggests that the introduction of appropriate internal energy into the compound is needed to release the stress at lithium insertion and to maintain the capacities during the repeating cycling.

Acknowledgements

This work was supported by a grant-in-aid for Scientific Research from the Ministry of Education, Culture, Sports, Science and Technology, and a grant from the Electric Technology Research Foundation of Chugoku and the Asahi Glass Foundation.

References

[1] A.N. Dey, J. Electrochem. Soc. 118 (1971) 1547.
[2] D. Fauteux, R. Koksbang, J. Appl. Electrochem. 23 (1993) 1.
[3] J.O. Besenhard, J. Yang, M. Winter, J. Power Sources 68 (1997) 87.
[4] R.A. Huggins, R. Koksbang, J. Power Sources 81/82 (1999) 13.
[5] Y. Idota, T. Kubota, A. Matsufuji, Y. Maekawa, T. Miyasaka, Science 276 (1997) 1395.
[6] O. Mao, R.A. Dunlap, J.R. Dahn, J. Electrochem. Soc. 146 (1999) 405.
[7] O. Mao, J.R. Dahn, J. Electrochem. Soc. 146 (1999) 414.
[8] O. Mao, J.R. Dahn, J. Electrochem. Soc. 146 (1999) 423.
[9] K.D. Kepler, J.T. Vaughey, M.M. Thackeray, Electrochem. Solid State Lett. 2 (1999) 307.
[10] K.D. Kepler, J.T. Vaughey, M.M. Thackeray, J. Power Sources 81/82 (1999) 383.
[11] D. Larcher, L.Y. Beaulieu, D.D. MacNeil, J.R. Dahn, J. Electrochem. Soc. 147 (2000) 1658.
[12] Y. Xia, T. Sakai, T. Fijieda, M. Wada, H. Yoshinaga, Electrochem. Solid State Lett. 4 (2001) A9.
[13] J. Yang, Y. Takeda, N. Imanishi, O. Yamamoto, J. Electrochem. Soc. 146 (1999) 4009.
[14] J. Yang, Y. Takeda, N. Imanishi, J.Y. Xie, O. Yamamoto, Solid State Ionics 133 (2000) 189.
[15] J. Yang, Y. Takeda, N. Imanishi, T. Ichikawa, O. Yamamoto, Solid State Ionics 135 (2000) 175.
[16] R. Alcantara, F.J. Fernandez-Madrigal, P. Lavela, J.L. Tirado, J.C. Jumas, J.C. Olivier-Fourcade, J. Mater. Chem. 9 (1999) 2517.
[17] D. Larcher, L.Y. Beaulieu, O. Mao, A.E. George, J.R. Dahn, J. Electrochem. Soc. 147 (2000) 1703.
[18] G.S. Cao, X.B. Zhao, T. Li, C.P. Lu, J. Power Sources 94 (2001) 102.
[19] X.B. Zhao, G.S. Cao, C.P. Lv, L.J. Zhang, S.H. Hu, T.J. Zhu, B.C. Zhou, J. Alloys Comp. 315 (2001) 265.
[20] H. Kim, J. Choi, H.-J. Sohn, T. Kang, J. Electrochem. Soc. 146 (1999) 4401.
[21] H. Sakaguchi, T. Esaka, Hyomen (Surface in Japanese) 39 (2001) 239.
[22] A. Saito, T. Horiba, Y. Aono. The 36th Battery Symposium in Japan, Abstr. 2B07 (1995).
[23] H. Sakaguchi, H. Honda, T. Esaka, Denki Kagaku (presently Electrochemistry) 66 (1998) 1291.
[24] H. Sakaguchi, H. Honda, T. Esaka, J. Power Sources 81/82 (1999) 224.
[25] H. Sakaguchi, H. Honda, H. Maeta, T. Esaka, Jpn. Inst. Metals Proc. 12 (1999) 1305.
[26] H. Honda, H. Sakaguchi, T. Fukunaga, T. Esaka, Electrochemistry 70 (2002) 99.
[27] H. Sakaguchi, H. Maeta, M. Kubota, H. Honda, T. Esaka, Electrochemistry 68 (2000) 632.
[28] H. Kim, Y.-J. Kim, D.G. Kim, H.-J. Sohn, T. Kang, Solid State Ionics 144 (2001) 41.
[29] J.T. Vaughey, C.S. Johnson, A.J. Kropf, R. Benedek, M.M. Thackeray, H. Tostmann, T. Sarakonsri, S. Hackney, L. Fransson, K. Edstrõm, J.O. Thomas, J. Power Sources 97/98 (2001) 194.
[30] K.C. Hewitt, L.Y. Beaulieu, J.R. Dahn, J. Electrochem. Soc. 148 (2001) A402.
[31] M. Maxfield, T.R. Jow, S. Gould, M.G. Sewchock, L.W. Shacklette, J. Electrochem. Soc. 135 (1988) 299.